Microchim Acta (2014) 181:1529–1539
DOI 10.1007/s00604-014-1219-4

ORIGINAL PAPER

Hybrid fluorescent nanoparticles fabricated from pyridine-functionalized polyfluorene-based conjugated polymer as reversible pH probes over a broad range of acidity-alkalinity

Haijun Cui · Ying Chen · Lianshan Li · Yishi Wu · Zhiyong Tang · Hongbing Fu · Zhiyuan Tian

Received: 6 December 2013 / Accepted: 24 February 2014 / Published online: 16 March 2014

Abstract Conjugated polymer nanoparticles (CPNs) were developed based on a polyfluorene-based conjugated polymer with thiophene units carrying pyridyl moieties incorporated in the backbone of polymer chains (PFPyT). Hybrid CPNs fabricated from PFPyT and an amphiphilic polymer (NP1) displayed pH-sensitive fluorescence emission features in the range from pH 4.8 to 13, which makes them an attractive nanomaterial for wide range optical sensing of pH values. The fluorescence of hybrid CPNs based on chemically close polyfluorene derivatives without pyridyl moieties (NP3), in contrast, remains virtually unperturbed by pH values in the same range. The fluorescence emission features of NP1 underwent fully reversible changes upon alternating acidification/basification of aqueous dispersions of the CPNs and also displayed excellent repeatability. The observed pH sensing properties of NP1 are attributed to protonation/deprotonation of the nitrogen atoms of the pyridine moieties. This, in turn, leads to the redistribution of electron density of pyridine moieties and their participation in the π-conjugation within the polymer main chains. The optically transparent amphiphilic polymers also exerted significant influence on the pH sensing features of the CPNs, likely by acting as proton sponge and/or acid chaperone.

Keywords Conjugated polymer nanoparticles · Fluorescence · pH sensing · Protonation

H. Cui · Y. Chen · Z. Tian (✉)
School of Chemistry & Chemical Engineering, University of Chinese Academy of Sciences (UCAS), Beijing 100049, China
e-mail: zytian@ucas.ac.cn

H. Cui · Y. Chen · L. Li (✉) · Z. Tang
Laboratory for Nanomaterials, National Center for Nanoscience and Technology, Beijing 100190, China
e-mail: lils@nanoctr.cn

Y. Wu (✉) · H. Fu
Beijing National Laboratory for Molecular Science (BNLMS), State Key Laboratory for Structural Chemistry of Unstable and Stable Species, and Key Laboratory for Photochemistry, Institute of Chemistry, Chinese Academy of Sciences, Beijing 100190, China
e-mail: yswu@iccas.ac.cn

Introduction

Acidity/alkalinity (pH) is undoubtedly one of the most important parameters in chemical, biological and environmental aspects [1–3]. For example, intracellular pH plays a vital role in organisms by exerting drastic influence on constituents such as cells, enzymes, and proteins, as well as organizational units such as muscles and nervous systems. Thus, accurately determining the local pH within a subcellular organelle is a prerequisite to taking insight into the physiological processes that take place in these small volumes, which represents a challenge to biology, physiology and medicine. Various kinds of pH sensors have been developed and successfully used in many fields [4, 5]. Among the various sensing schemes, there has been burgeoning interest in exploiting pH sensing with fluorescence signaling because such signaling way inherently enables ultrahigh sensitivity, produces excellent spatiotemporal resolution, and can be easily manipulated [6, 7]. Various fluorescent reporters such as fluorescent proteins (FPs), quantum dots (QDs), and small-molecular-weight organic dyes were used as probes for pH sensing and each type of probe definitely demonstrates its advantages but also has apparent limitations [8–12]. FPs are undoubtedly biocompatible and can be easily integrated with biological proteins and thus eliminate the need for exogenous probes to target to specific protein. However, FPs are generally much dimmer as compared to most small-molecular-weight organic fluorophores.

Additionally, low photobleaching thresholds also make FPs more vulnerable to light illumination and consequently not suitable for an extended period of monitoring. QDs are typically characterized with the tunable fluorescence, narrow emission, high fluorescence quantum yield and photobleaching threshold; but are generally either toxic or interfere with biological activities, including non-specific bind to biomolecules [13, 14]. Small-molecular-weight organic dyes have flexible structures and fluorescence emission features but generally suffer from poor photostability [15, 16].

In comparison to these abovementioned fluorescent reporters, fluorescent conjugated polymers nanoparticles (CPNs) are characterized with large absorption cross section, high fluorescence quantum yield, excellent photostability and biocompatibility [17–19]. The past decade has witnessed the emergence and increasing advancements of CPNs as novel types of probes for biological fluorescence detection applications owing to their salient features, such as relatively high brightness, absorption cross sections, and good photostability [20, 21]. Specifically, as efforts to take advantage of these feature-packed conjugated polymer nanoparticles (CPNs), CPNs were recently exploited as fluorescent sensors for pH sensing on the basis of Förster resonance energy transfer (FRET) mechanism [22]. Activating FRET between two chromophores requires the absorption band of the energy acceptor to overlap properly with the emission band of the energy donor. In addition, FRET efficiency remains essentially zero unless the donor and acceptor are within or near the Förster distance. These stringent requirements definitely complicate the design and construction of FRET-based pH sensors and impose an uncontrollable influence on the pH-sensitive fluorescence signal of the sensors. Apparently, approaches to circumvent these requirements and therefore optimize the pH sensing mechanism are critically needed. In the present work, a new type of CPNs-based pH sensors was developed from newly synthesized polyfluorene derivatives with thiophene units carrying pyridyl moieties incorporated in the backbone of polymer chains (PFPyT). Hybrid CPNs fabricated from fluorescent PFPyT and optically transparent amphiphilic polymer carrying sulfonic acid moieties (PS-SO_3H) clearly displayed pH-sensitive fluorescence emission over a wide pH range from 4.8 to 13. Specifically, the amphiphilic polymer component played a vital role in the pH sensing features of the hybrid CPNs. The pH sensing ability of the as-prepared CPNs is attributable to the reversible protonation/deprotonation of nitrogen atoms of pyridine moieties. Thus, such new type of CPNs-based pH sensor displayed pH sensing features with one type of fluorophore involved and no FRET is needed.

Experimental section

Materials

3-Thienylboronic acid, Tetrahydrofuran (UV, HPLC Grade, min. 99.7 %) was purchased from Alfa-Aesar Co. (www.alfa.com) 3-Bromopyridine, 9, 9-Dioctylfluorene-2, 7-diboronic acid bis (1, 3-propanediol) ester (monomer **1**), 2,5-Dibromothiophene (monomer **3**), Tetrakis (triphenylphosphine)palladium(0) [$Pd(PPh_3)_4$], Aliquat® 336, Polystyrene-*block*- poly(ethylene-*ran*-butylene)-*block*-polystyrene, sulfonated solution (PS-SO_3H) (5 wt. % in 1-propanol and dichloroethane) were purchased from Sigma-Aldrich Co. (www.sigmaaldrich.com/china-mainland.html) 7-Diethylamino-4-methylcoumarin, 99 % (coumarin 1) was obtained from J&K Co. (www.jkchemical.com) All other chemicals were from commercial sources and of analytical reagent grade, unless indicated otherwise.

Apparatus

UV–vis absorption spectra were recorded on Hitachi U-3010 spectrophotometer (www.hitachi-hitec.com). FluoroMax 4 spectrofluometer (Horiba Jobin Yvon, www.horiba.com) was used to measure fluorescence spectra. The pH adjustments were confirmed by a pH meter (METTLER TOLEDO FE20K, www.mt.com), which was calibrated with buffers of pH=4.00, 6.86, and 9.18 at room temperature. ^{1}H NMR and ^{13}C NMR spectra were recorded on Bruker Avance 400 M (www.bruker.com). The Milli-Q water (18.2 MΩ·cm at 25 °C) was used as deionized water by Millipore Co. (www.millipore.com) The molecular weight of polymer was confirmed by gel permeation chromatography (GPC 40, THF, polystyrene standard, 40 °C, Agilent Co. www.agilent.com). The average sizes and size distributions of polymer nanoparticles were characterized by dynamic light scattering (Zetasizer Nano ZS, Malvern Instruments Ltd, www.malvern.com).

Synthesis of 3-(2-pyridyl) thiophene [23]

3-Thienylboronic acid (0.976 g, 7.63 mmol), 3-Bromopyridine (1.00 g, 6.36 mmol), K_2CO_3 (4.38 g, 31.7 mmol), a few droplets Aliquat® 336, 30.0 mL water and 30.0 mL THF were placed into a 100 mL Schlenk tube. The tube degassed by three freeze-pump-thaw cycles, and backfilled with argon. Then the mixture were transferred to a new Schlenk tube with $Pd(PPh_3)_4$ (0.22 g, 0.19 mmol). Under vigorous stirring, the mixture was kept at 60 °C for 24 h. After which the reaction was cooled to room temperature and poured into 200 mL of cold water. The mixture was extracted with dichloromethane. The organic phase was washed with water, dried over anhydrous magnesium sulfate and evaporated

to give a crude product. The dark brown crude product was further purified by silica gel column, using DCM as eluent. Light yellow solid (0.93 g) was obtained to give a yield of 95 %.^{1}H NMR (400 MHz, $CDCl_3$): δ 8.88 (Py-H, 1H), δ 8.54 (Py-H, 1H), δ 7.88 (Py-H, 1H), δ 7.53 (Th-H, 1H), δ 7.46 (Th-H, 1H), δ 7.41 (Py-H, 1H), δ 7.34 (Py-H, 1H).

Synthesis of 2, 5-dibromo-3-(2-pyridyl) thiophene (monomer **2**) [23]

A 100 mL round bottom flask was filled with 3-(2-pyridyl) thiophene (1.52 g, 9.8 mmol), sodium acetate (3.11 g) and acetic acid (28 mL). And a solution of bromine (5.1 g, 30.0 mmol) and acetic acid (19 mL) was added dropwise to the flask. The mixture was refluxed for 4 h and cooled to room temperature. The mixture was poured into 200 mL cold water and neutralized to pH 7–8 by adding sodium carbonate. Then it was successively extracted with THF and diethyl ether. The combined organic layers were washed with water, dried over anhydrous magnesium sulfate and evaporated to give a crude product. After purification by silica gel column (heptane/ethyl acetate=4:1 as eluent), a white powder was obtained (1.98 g, 66 %). ^{1}H NMR (400 MHz, $CDCl_3$): δ 8.76 (Py-H, 1H), δ 8.62 (Py-H, 1H), δ 7.85 (Py-H, 1H), δ 7.38 (Py-H, 1H), δ 7.04 (Th-H, 1H).

Synthesis of poly [2, 7-(9, 9-dioctylfluorene) -co-alt-2, 5-(2-pyridyl) thiophene] (PFPyT)

A mixture of K_2CO_3 (552.76 mg, 4 mmol), a few droplets Aliquat® 336, 2.0 mL water and 3.0 mL toluene were placed into a 10 mL Schlenk tube. The tube degassed by three freeze-pump-thaw cycles, and backfilled with argon. Another tube loaded with monomer **1** (182.6 mg, 0.327 mmol), monomer **2** (104.3 mg, 0.327 mmol), and $Pd(PPh_3)_4$ (30 mg, 0.0246 mmol) was prepared in the glove box. Then, the degassed solution was transfer into the new tube. The mixture was stirred at 80 °C for 2 days under argon atmosphere. After which the reaction was cooled to room temperature and precipitated into 200 mL of cold methanol. The product was recovered by filtration, loaded into a Soxhlet thimble, and washed with methanol (6 h), acetone (24 h) to remove oligomers and catalyst residues. The resulting polymers were collected and dried under vacuum. 112 mg greenish solid was obtained to give a yield of 62 %. ^{1}H NMR (400 MHz, $CDCl_3$): δ 8.75, 8.53, 7.75-7.41, 7.18-7.14, 2.07, 1.93, 1.80, 1.68, 1.26-1.06, 0.92-0.50. ^{13}C NMR (400 MHz, $CDCl_3$): δ 151.95, 151.43, 149.90, 148.13, 143.90, 140.43, 139.99, 136.43, 135.35, 132.74, 128.19, 125.62, 124.73, 123.73, 123.11, 120.43, 120.23, 119.82, 55.27, 40.32, 31.84, 30.01, 29.72, 29.40, 29.31, 29.23, 23.75, 22.64, 14.09, 1.04, 0.01.GPC (THF, polystyrene standard): M_n=15,352, M_w=29,469, PDI=1.92.

Synthesis of poly [2, 7-(9, 9-dioctylfluorene) -co-alt-2, 5-thiophene] (PFT)

The PFT polymer was synthesized according to the literature [24]. ^{1}H NMR (400 MHz, $CDCl_3$): 7.80-7.00, 2.18-2.04, 1.58, 1.26, 1.09, 0.82-0.60. GPC (THF, polystyrene standard): M_n=9,899, M_w=23,067, PDI=2.33.

Preparation of CPNs aqueous samples

The water dispersed CPNs were prepared by using a reprecipitation method according to the literature. In a typical protocol, PFPyT or PFT (0.1 mg) and PS-SO_3H (2 mg) were dissolved in THF (1 mL). The mixture was kept in dark overnight to form a homogeneous solution. Then the solution mixture was quickly added into a meticulously clean vial with 10 mL of deionized water under continuous sonication. The THF was removed by partial vacuum evaporation at 45 °C. Finally, the aqueous solution was filtered through a 0.22 μm PTFE syringe driven filter. The bright obtained nanoparticle solution was stored in dark at room temperature. For the adjustments of the pH of CPNs aqueous dispersion in the present work, sodium hydroxide and hydrochloric acid aqueous solution with different concentrations (4, 2, 0.4, 0.2, 0.04, 0.02, 0.002 M) were used to gain a certain pH. And pH value was confirmed by pH meter which was calibrated before use (slope: 98 %).

Results and discussion

Polyfluorene and its derivatives have expressed excellent photoelectrical properties. “A-B” type polyfluorene derivatives investigated in the present work were synthesized via Suzuki polymerization strategy. Fluorescent conjugated polymers PFPyT and PFT used in the present work were synthesized via typical Pd-catalyzed Suzuki coupling reactions according to literature with the synthetic routes illustrated in Scheme 1. Specifically, 9, 9-dioctylfluorene-2, 7-diboronic acid bis (1, 3-propanediol) ester was used as the common building block for the Suzuki polymerization, which coupled with 2, 5-dibromothiophene carrying pyridyl moieties, yielding the target conjugated polymer (PFPyT) as a greenish solid. Replacing 2, 5-dibromothiophene carrying pyridyl moieties with 2, 5-dibromothiophene, another target polymer with similar structure, PFT, was also obtained. The as-synthesized conjugated polymers were characterized by ^{1}H, ^{13}C NMR spectroscopy and GPC. PFPyT and PFT have good solubility in common organic solvent, such as tetrahydrofuran (THF), chloroform, toluene, chlorobenzene, but precipitate in highly polar solvents, such as methanol and ethanol. In chloroform solution, PFPyT exhibited a broad absorption band spanning from 320 to 470 nm with the absorption maximum at 409 nm,

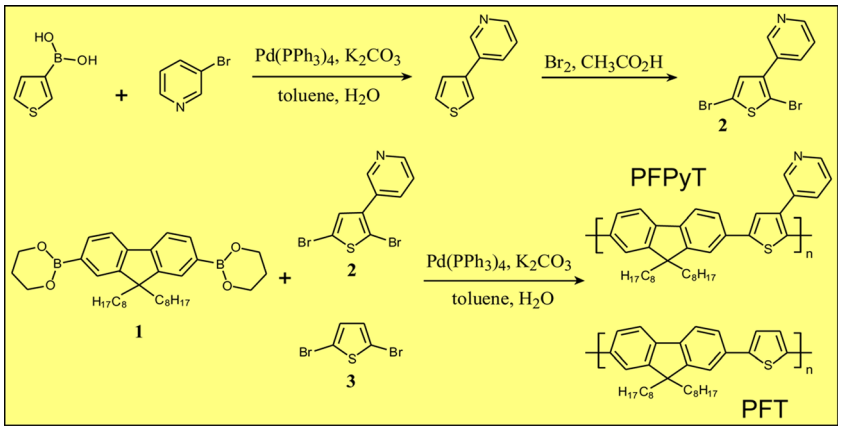

Scheme 1 Synthesis of monomers and the target fluorescent conjugated polymers PFPyT and PFT via Suzuki coupling

as shown in Fig. 1. Upon excitation at 409 nm, PFPyT in chloroform showed a broad emission band in the range of 420 to 650 nm, with peak at 468 nm and two shoulders around 496 nm and 534 nm originating from the vibronic structures of the polymer. PFT in chloroform displayed a broad absorption peak with maximum of 434 nm and an onset of 500 nm, showing a ~25 nm red-shift compared to the absorption features of PFPyT in chloroform. The photoluminescence spectrum of PFT in chloroform also displayed vibronic features similar to those of PFPyT, showing distinct emission peaks at 474, 500 nm and a shoulder around 540 nm.

Conjugated polymer materials exhibit attractive optical features, such as high fluorescence quantum yield, large extinction coefficients, and efficient energy-transfer properties, which meets the technical requirements as probes for many biological applications to a great extent. With these advantageous properties, conjugated polymers have already drawn ever-increasing attention to exploiting new class of fluorescent probes and considerable progress have been made in recent years. Specifically, fluorescent nanoparticles based on various π-conjugated polymers have been developed as probes for fluorescence detection owing to their salient features including relatively high brightness, large absorption cross sections, and good photostability. In the present work, conjugated polymer nanoparticles (CPNs) based on the as-synthesized PFPyT and PFT polymers were prepared via reprecipitation method. Specifically, fluorescent conjugated polymers PFPyT and PFT were used as the photoactive components and the amphiphilic polymer PS–SO_3H was used to decorate the surfaces of the CPNs [25, 26]. For instance, to prepare CPNs containing PFPyT and PS–SO_3H (NP1), PFPyT and PS-SO_3H were premixed in THF overnight and the as-prepared polymer solution was then used for reprecipitation. PS–SO_3H polymers consist of hydrophobic alkyl main chains and side chains bearing hydrophilic sulfonated styrene units. Thus during the reprecipitation process, the hydrophobic alkyl main chains of PS–SO_3H are prone to entwine with PFPyT main chains due to hydrophobic interactions in aqueous media, and therefore form a hydrophobic core, while the hydrophilic side chains of PS–SO_3H reside on the surfaces of the polymer NPs, as

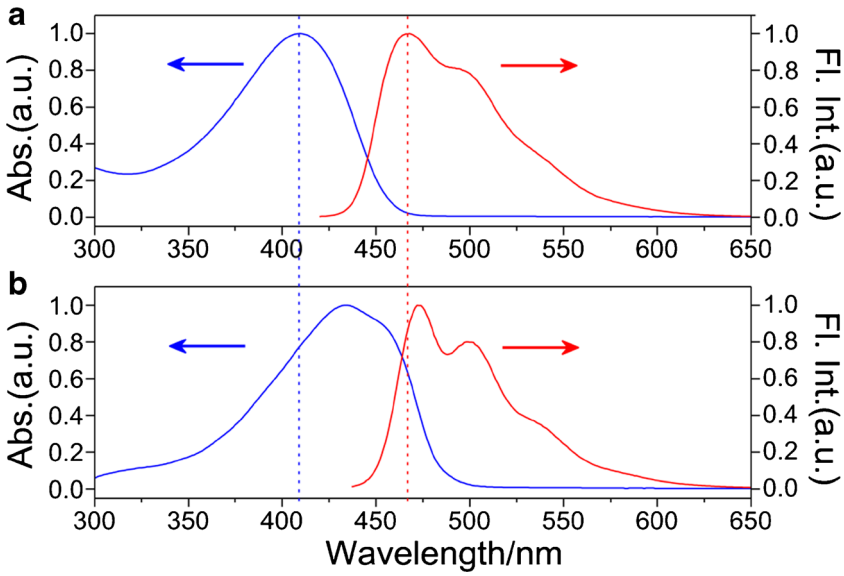

Fig. 1 Normalized absorption (*blue solid line*) and fluorescence emission spectra (*red solid line*) of the conjugated polymers PFPyT (**a**) and PFT (**b**) in chloroform

illustrated in Scheme 2, making the as-prepared CPNs suspensible in aqueous solution. Dynamic light scattering (DLS) measurement of the sample reports an average hydrodynamic diameter of ~29 nm and a relatively narrow polydispersity. Additionally, the as-prepared bright and light yellow CPNs dispersion were stored at room temperature without noticeable aggregation, suggesting the excellent stability of the samples.

Figure 2 displays the UV–Vis absorption and fluorescence emission properties of NP1 aqueous dispersion at different pH values. For the UV–Vis absorption spectra, the shape of the absorption spectra nearly kept unchanged but obvious redshift was clearly observed upon increasing the alkalinity of the aqueous solution, as shown in Fig. 2a. Specifically, upon changing the pH of the aqueous solution from 4.8 to 13, the absorption maximum of the NP1 aqueous dispersion shifted from 402 to 417 nm (Fig. 2b). In contrast to the changes in the UV–Vis absorption spectra, remarkable changes in the fluorescence emission spectra of the NP1 aqueous dispersion sample, both in shape and intensity, were observed upon changing the pH of the sample, as shown in Fig. 2c. Upon excitation at 405 nm, the initial NP1aqueous dispersion sample exhibited a broad structureless emission band centered at ~533 nm. It is noted that the pH value of the initial NP1 aqueous dispersion was 4.8. To evaluate the pH sensing performance of the as-prepared NP1 aqueous dispersion sample, dilute sodium hydroxide solution was added into the sample to tune the acidity/alkalinity of the sample and then the fluorescence spectra were acquired after the solution reaches equilibrium. As shown in Fig. 2c, increasing the pH from 4.8 up to 5.2 gave rise to the emergence of two emission peaks at 477 and 508 nm, respectively, and these two emerging peaks gradually become prominent upon further incremental increase in the basicity of the aqueous dispersion sample. Of note, the fluorescence emission spectrum of NP1 in moderate and strong alkaline aqueous environment clearly displays one peak (477 nm) and two shoulders (508, 533 nm), highly resembling the fluorescence emission spectrum of PFPyT/chloroform solution in shape, indicating that PFPyT components remained their identities after reprecipitation together with PS-SO_3H in aqueous milieu. Figure 2d shows a plot of $(I\text{-}I_0)/I_0$ against the pH value of the aqueous milieu ranging from 4.8 to 13, where I_0 and I represent the fluorescence intensity (at 477 nm) of the initial NP1 aqueous dispersion sample (pH=4.8) and that of the same sample at other pH values, respectively. It can be seen that the fluorescence intensity of the NP1 dispersion sample clearly displayed dependence on the pH value of the aqueous milieu, indicating the pH sensing ability of the as-prepared CPNs. The pH value was also found to remarkably affect fluorescence quantum yield (ϕ_F) of the NP1 dispersion sample. Specifically, a quantum yield of ϕ_F=~0.61 was determined for the PFPyT/THF solution when compared to coumarin 1 in ethanol (ϕ_F=~0.73); NP1 dispersion sample in pH 4.8 environment acquire a poor quantum yield of ϕ_F=~0.02 while increasing the pH value of the sample up to 13 resulted in a quantum yield of ϕ_F=~0.13. In contrast, the DLS measurements showed that change in pH value did not exert significant influence on the size of the as-prepared NP1 aqueous dispersion sample, as shown in Fig. 3, suggesting the stability of the nanoparticles during the of acidification and basification processes. Based on the characterization results of three batches of NP1 sample prepared via the identical protocol, DLS measurements presented acceptable variation in average size while the pH ranges and fluorescence quantum yields of the sample were found nearly reproducible.

Figure 4 displays the repeatability of the fluorescence emission features of NP1 aqueous dispersion upon alternating changing the pH value of the aqueous milieu of the sample between 5 and 11. Specifically, the pH value was adjusted to and fro between 5 and 11 by using hydrochloric acid and sodium hydroxide solutions. It can be seen that the initial NP1 aqueous dispersion sample with pH of 5 fluoresces weakly in a broad range spanning from 425 to 700 nm with emission maximum at ~533 nm. Upon increasing pH value of the sample up to 11, the emission intensity significantly increases, with the concomitant changes in the spectrum shape from a structureless broad band to a blue-shifted band with

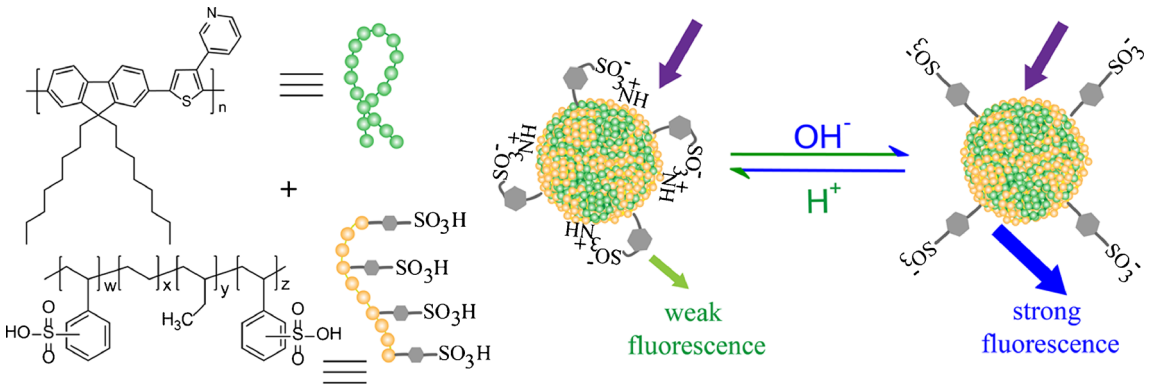

Scheme 2 Preparation of hybrid polymer nanoparticles (NP1) and illustration showing the reversible response of NP1 to acidification/basification

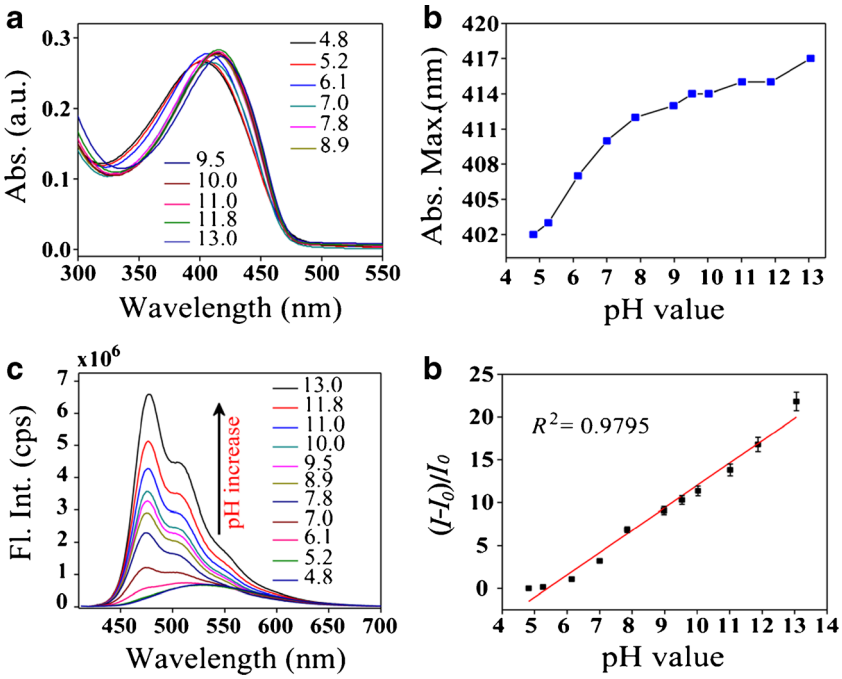

Fig. 2 **a** UV–Vis absorption spectra and **b** the corresponding absorption peaks of NP1 aqueous dispersion with different pH values (concentration of NP1 is 0.01 mg·mL^{-1} in water). **c** Fluorescence emission spectra (λ_{ex}=405 nm) of NP1 aqueous dispersion with different pH values. **d** A plot of the ratio of I-I_0 over I_0 as a function of the pH value of the aqueous milieu, where I_0 and I represent the fluorescence intensity (at 477 nm) of the initial NP1 aqueous dispersion sample (pH=4.8) and that of the same sample at other pH values, respectively. The *scattered symbols* represent experimental data and the *red solid line* is linear fit of the data

vibronic fine structures, as shown in Fig. 4a. Additionally, upon tuning the pH value back to 5, the fluorescence intensity nearly completely recovered and the emission spectrum shape faithfully restored from the band with vibronic fine structures to the one with broad structureless band. The following basification/acidification cycle under sequential addition of sodium hydroxide and hydrochloric acid solution also demonstrated the recoverability of the fluorescence emission features of NP1 aqueous dispersion sample, as shown in Fig. 4b. Furthermore, such recoverability of the fluorescence emission upon basification/acidification stimuli provides a clue of the involvement of a pH-dependent reversible process, as discussed in the next section.

To evaluate the acidity sensing features of conjugated polymer PFPyT in nonaqueous solvent milieu, fluorescence emission spectra of PFPyT/$CHCl_3$ solution at the absence and presence of four types of typical organic acids, namely, camphorsulfonic acid (CSA), trifluoroacetic acid (TFA), dichloroethanoic acid (DCA), and dodecyl benzenesulfonic acid (DBSA), respectively, were acquired as shown in Fig. 5. Upon addition of two equivalent organic acids, the absorption maximum of the PFPyT/$CHCl_3$ solution clearly displayed

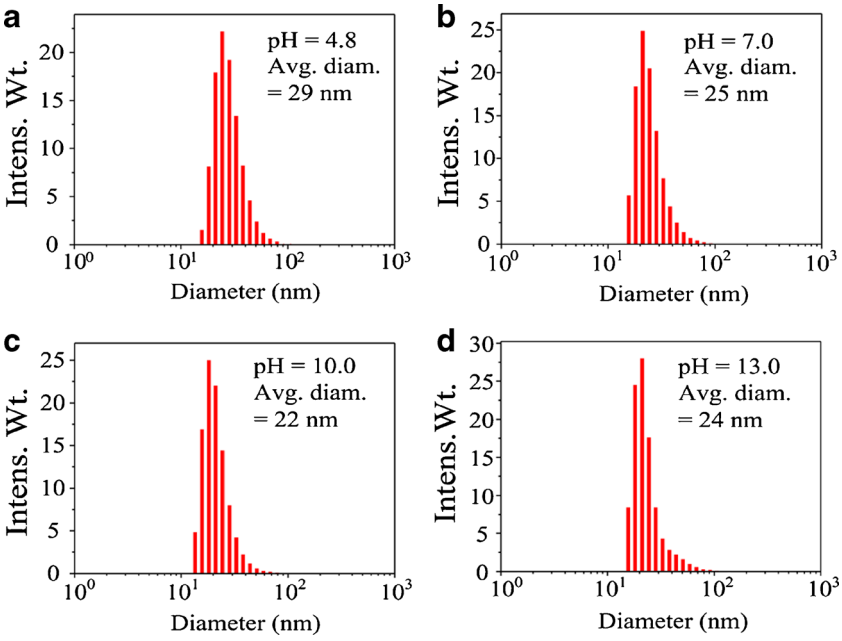

Fig. 3 DLS measurement results of the as-prepared NP1 aqueous sample at pH of 4.8, 7.0, 10.0, and 13

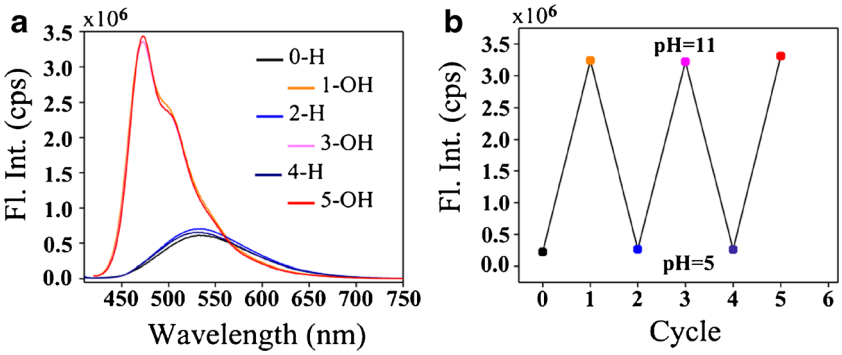

Fig. 4 **a** Fluorescence emission spectra of NP1 aqueous dispersion under alternating cycles of changing the pH value of the aqueous milieu of the sample between 5 and 11. **b** Evolution of fluorescence intensity (at 477 nm) of NP1 aqueous dispersion sample with alternating cycles of pH value of 5 and 11

blue-shift from 409 nm to 398 nm in the cases of CSA and DBSA and to 395 nm in the cases of TFA and DCA. Of note, such organic acids induced absorption spectra blue-shifts of PFPyT/$CHCl_3$ solution are in line with the changes observed in the PFPyT-based CPNs aqueous dispersion sample. At the presence of organic acids, protonation of the nitrogen atoms of the pendant pyridyl group eliminates its electron-releasing character and corresponding charge transfer, and thus contributing to the shift of absorption band to high-energy region [27]. For the fluorescence emission spectrum of PFPyT/$CHCl_3$ solution, addition of organic acids leads to remarkable decrease in the fluorescence intensity, as shown in Fig. 5b. It is proposed that protonation of the nitrogen atom of the pendant pyridyl group eliminates its electron-releasing character and thus reduces its participation in the π-conjugation of the conjugated backbone [28, 29]. Additionally, such acidification gives rise to an obvious change in the spectrum shape, namely, from emission band with vibronic fine structure to structureless broad band. Such loss of vibronic fine structure in fluorescence emission spectrum upon acidification was also observed in the case of PFPyT-based CPNs aqueous dispersion sample, which might be a result of the protonation of pendant pyridyl group [30].

In order to explore the role of amphiphilic polymer PS-SO_3H in the pH sensing of NP1 sample, neat PFPyT CPNs (NP2), namely, without the involvement of PS-SO_3H component, was prepared via reprecipitation strategy and their pH sensing properties were investigated. Of note, the as-prepared NP2 aqueous dispersion is nearly neutral (pH close to 7) and displays fluorescence emission peak around 474 nm, in contrast to pH 4.8 and the 533-nm emission peak of the initial NP1 aqueous dispersion sample. As shown in Fig. 6, acidification of the neutral NP2 aqueous dispersion leads to remarkable decrease in the fluorescence intensity, similar to the changes observed in the NP1 aqueous dispersion. Interestingly, no noticeable changes in the fluorescence spectrum was observed upon basification of the initial neutral NP2 aqueous dispersion, in sharp contrast to the responding features of NP1 aqueous dispersion in the same pH range. Such difference in the pH sensing performance between NP1 and NP2 aqueous dispersion samples suggests that PS-SO_3H exerts definite effects on the pH sensing features of the CPNs in the present work. For the as-prepared CPNs containing PFPyT and PS-SO_3H, namely NP1, the surface-bound benzenesulfonic acid groups have a pKa ~3 and therefore enable acidification/protonation of the pyridyl moieties of PFPyT component.

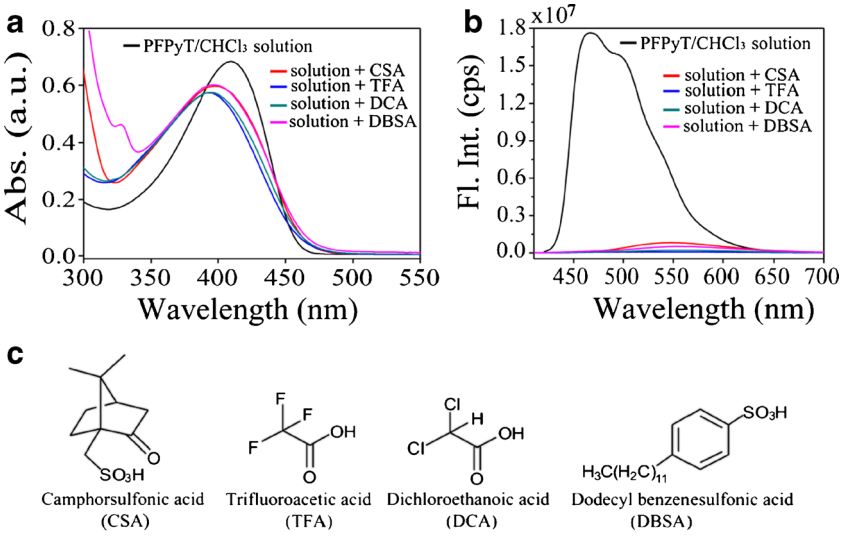

Fig. 5 **a** UV–Vis absorption spectra and **b** fluorescence emission spectra (λ_{ex}=405 nm) of PFPyT/$CHCl_3$ solution and PFPyT/$CHCl_3$ solution with additional two equivalent organic acids. **c** Chemical structures of four organic acids

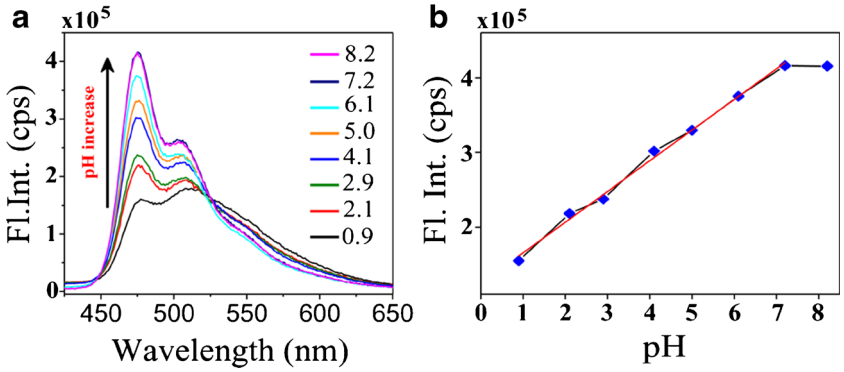

Fig. 6 **a** Fluorescence emission spectra (λ_{ex}=405 nm) of NP2 aqueous dispersion with different pH values. **b** Fluorescence intensity (at 474 nm) of NP2 aqueous dispersion as a function of the pH value of the aqueous milieu

Obviously, difference in the acidity levels between NP1 and NP2 aqueous samples, namely pH 4.8 versus pH ~7.0, provides a coherent picture of such acidification of the pyridyl moieties. Additionally, the fluorescence emission features of the initial CPNs aqueous dispersion samples containing NP1 and NP2, respectively, also echo the protonation of the pyridyl moieties of PFPyT component, namely the initial NP1-containing aqueous dispersion sample (pH 4.8) exhibit a broad structureless emission band centered at ~533 nm while the NP2-containing counterpart clearly display blue-shifted emission band with vibronic fine structures (Fig. 6a). Another noteworthy distinct difference between the NP1-containing aqueous dispersion sample and its NP2 counterpart is their responses to pH change in the basic environment. Upon increasing pH from 7 up to 13, the fluorescence intensity of NP1 sample remarkably increases while that of NP2 sample nearly keeps unperturbed, as shown in Figs. 2 and 6. The most likely explanation for such observed discrepancy resides with the role of proton sponge or acid-chaperone that PS-SO_3H groups play in the hybrid NP1 CPNs. In alkaline milieu, benzenesulfonic acid groups likely release proton in a cooperative way with the pyridine moieties and the interactions between the benzenesulfonic acid groups and pyridine moieties possibly vary upon changing the alkalinity levels, exerting influence on the response of NP1 to pH change.

To gain insight into the vital role of pyridine moieties in the pH sensing performance of NP1 sample, another polyfluorene-based conjugated copolymer without pyridine moieties, PFT, was synthesized and the corresponding hybrid CPNs containing PFT and PS-SO_3H (NP3) was fabricated. Figure 7 displays the UV–Vis absorption and fluorescence emission spectra of NP3-containing aqueous dispersion sample with different acidity levels. It can be clearly seen that neither the absorbance nor the fluorescence spectra show noticeable change upon changing pH values in the range of 1 to 10, indicating independence of spectral features of NP3 sample on the change in the acidity/alkalinity of the aqueous milieu. Undoubtedly, such stark contrast in fluorescence response to pH change between NP3 and NP1 clearly demonstrates the vital role of pyridine moieties in the pH sensing ability of NP1-based CPNs sample. Specifically, pyridine moieties undergo protonation/deprotonation processes upon acidification/basification, which contribute to the sensitive response in fluorescence emission features of the CPNs fabricated from the conjugated polymer possessing pyridine moieties. Additionally, the protonation/deprotonation processes of pyridine moieties are reversible, which inherently enables the recoverability of fluorescence emission features of NP1 CPNs upon multiple cycles of pH change, as illustrated in Fig. 4.

To explore information regarding the excited state behavior of NP1, transient fluorescence spectroscopy measurements of NP1 samples in aqueous milieu with different acidities were carried out. Figure 8 illustrates the picosecond time-resolved fluorescence decay curves of NP1 aqueous dispersion sample with pH 7 and pH 13, respectively. For these two NP1 aqueous dispersion samples, their transient fluorescence decay curves can be fit adequately with a bi-exponential function. Specifically, the decay curve of NP1 dispersion sample at

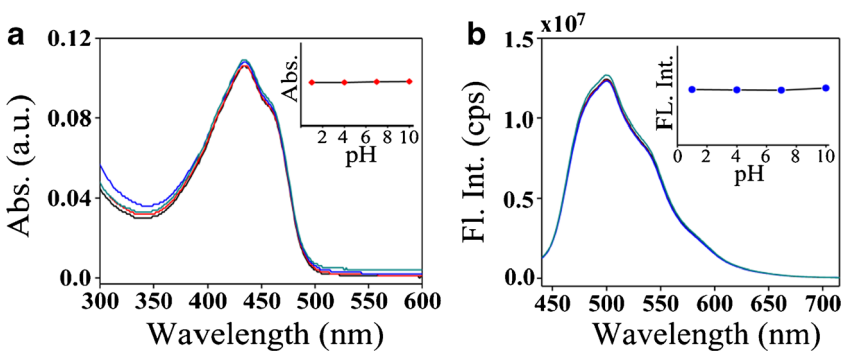

Fig. 7 UV–Vis absorption (**a**) and fluorescence emission spectra (**b**) of NP3 aqueous dispersion at pH=1, 4, 7, 10. Concentration of NP3 was 0.01 mg·mL^{-1} in water and the excitation wavelength was at 430 nm. Insert: absorption maximum (at 430 nm) and emission peak (at 500 nm) as a function of pH value of the sample

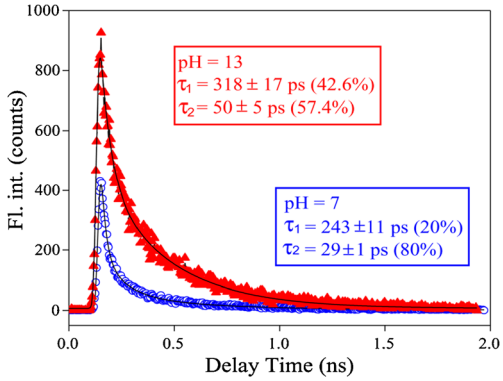

Fig. 8 Picosecond time-resolved fluorescence decay kinetics (at 477 nm) of NP1 aqueous dispersion sample at pH 7 (*blue open cycles*) and pH 13 (*solid triangle*). The *scattered symbols* represent experimental data and the *black solid lines* are fits. The temporal resolution was ~10 ps

pH 7 is well-resolved into two decay components with high accuracy, a long decay lifetime τ_1=243±11 ps (20 %) and a short lifetime τ_2=29±1 ps (80 %), respectively, which is consistent with the fluorescence lifetime results of CPNs constructed from conjugated polymers with similar chemical structures. From the decay curve of NP1 dispersion sample at pH 13, a long decay lifetime τ_1=318±17 ps (42.6 %) and a short lifetime τ_2=50±5 ps (57.4 %) are obtained. It can be seen that upon increasing pH from 7 up to 13, the fluorescence lifetime parameters of both the long-lifetime component and the short-lifetime component remarkably increase. Another noteworthy feature is that upon increasing pH from 7 up to 13, the population of the long-lifetime component significantly increases from 20 to 42.6 %. Owing to the increase in the fluorescence lifetimes of two components and the population of the long-lifetime component, increasing pH from 7 up to 13 leads to a significant increase in the average fluorescence lifetime of NP1 aqueous dispersion sample from 174 to 271 ps, suggesting a change in the excited state of the PFPyT fluorescent component in NP1. For NP1 aqueous dispersion sample, acidification of the sample is expected to protonate the pyridine moieties of PFPyT component and therefore prevent the lone pair of N atom from its participation in the π-conjugation with main chains. Conversely, basification of the sample brings about deprotonation of the pyridine moieties and therefore releases the sequestrated lone pair of N atom for π-conjugation, which is expected to enable more excited-state species to relax to the ground state via the way of photon emission. As a result, the prolonged fluorescence lifetime and enhanced fluorescence emission intensity of NP1 aqueous dispersion sample upon basification were observed.

Table 1 lists several types of typical nanomaterials as pH sensors. It can be seen that each kind of methods/materials has its specific features. As compared to other reported pH sensors, sensors developed in the present work exhibited pH sensing performance in a wider pH range and in a reversible way. More importantly, only protonation and deprotonation of single fluorophore species are involved in the reversible pH sensing processes of the sensors in the present work, thus circumventing the stringent requirements such as FRET, electron transfer, and combination of pH-sensitive fluorophores and pH-insensitive molecules that involved in other types of sensors.

Conclusion

In summary, a new type of fluorescent conjugated polymer with thiophene units carrying pyridyl moieties incorporated in the backbone of the polyfluorene chains were synthesized;

Table 1 Figures of merits of the typical nanomaterials as pH sensors

Methods/Materials used	Analytical ranges	Mechanism	Features	Ref.
Perylene bisimide vesicles loaded with bispryene	pH 3.0–11.0.	FRET	Bilayer vesicle systems showing pH-sensitive photo-functions	[31]
Ratiometric fluorescent nanogel for pH sensing	Physiological range (6–8)	FRET	pH-sensitive ratiometric fluorescence signaling	[32]
Dendrimer labeled with Coumarin, fluorescein, and Oregon green	Alkaline, neutral, and acidic for three sensors	Conjugation of pH-sensitive & pH-insensitive molecules	Targetable ratiometric pH sensors	[15]
QDs/dopamine bioconjugates	pH 4.0–9.0	Redox and electron-transfer	QD-dopamine-based intracellular pH sensing	[10]
CPNs doped with pH-sensitive dyes	pH 5.0–8.0	pH-sensitive FRET	Excellent reversibility and stability	[22]
Pyridine-containing small organic molecule	Acidity	Protonation-dependent AIE	Switching between blue and dark states	[33]
Dopamine-modified conjugated polymer	pH 5.0–9.0	Intramolecular electron transfer	Fluorescence "turn-on" response at low pH	[34]
Pyridine-containing CPNs	pH 4.8–13	Protonation and deprotonation	Reversible pH sensing over wide pH range	This work

FRET Förster resonance energy transfer, *AIE* aggregation-induced emission

hybrid CPNs consisting of such "A-B" type polyfluorene derivatives were fabricated via reprecipitation strategy and their pH sensing properties were investigated in the present work. CPNs fabricated from polyfluorene derivatives carrying the pyridyl moieties (NP1) clearly displayed pH-sensitive fluorescence emission features in the range of pH 4.8 to 13. Additionally, fluorescence intensity of such NP1 underwent reversible fluctuation upon alternating acidification/basification of the CPNs aqueous dispersion sample. In sharp contrast, fluorescence emission features of the hybrid CPNs based on the polyfluorene derivatives without the pyridyl moieties (NP3) were found nearly unperturbed upon pH change in the same range. Additionally, acidification/basification of NP1 aqueous dispersion sample brought about remarkable changes in the fluorescence lifetime of NP1, indicating the influence that the factor of acidity/alkalinity exerts on the excited-state behavior of NP1. It is believed that the observed pH sensing properties that NP1 displayed originate from the protonation/deprotonation of the nitrogen atoms of the pyridine moieties upon acidification/basification of the CPNs samples, which is expected to lead to the redistribution of electron density of pyridine moieties and their participation in the π-conjugation with polymer main chains. The amphiphilic polymer also exerted significant influence on the pH sensing features of the as-prepared CPNs, likely via the way of acting as proton sponge and/or acid chaperone.

Acknowledgments This work was supported by the National Natural Science Foundation of China (grant no. 21173262, 21373218) and the "Hundred-Talent Program" of CAS to Z. Tian.

References

1. Roos A, Boron WF (1981) Intracellular pH. Physiol Rev 61:296–434
2. Young BP, Shin JJH, Orij R, Chao JT, Li SC, Guan XL, Khong A, Jan E, Wenk MR, Prinz WA, Smits GJ, Loewen CJR (2010) Phosphatidic acid is a pH biosensor that links membrane biogenesis to metabolism. Science 329:1085–1088
3. Roy I, Gupta MN (2003) Smart polymeric materials: emerging biochemical applications. Chem Biol 10:1161–1171
4. Fog A, Buck RP (1984) Electronic semiconducting oxides as pH sensors. Sensors Actuators 5:137–146
5. Swindlehurst BR, Narayanaswamy R (2004) Optical sensing of pH in low ionic strength waters. In: Narayanaswamy R, Wolfbeis OS (ed) Optical sensors industrial environmental and diagnostic applications. Springer-Verlag, Berlin Heidelberg 12, pp 281–308
6. Johnson I, Spencer MTZ (2010) The molecular probes handbook, 11th edn. Life Technologies, California
7. Lakowicz JR (2006) Principles of fluorescence spectroscopy. Springer, Berlin
8. Krulwich TA, Sachs G, Padan E (2011) Molecular aspects of bacterial pH sensing and homeostasis. Nat Rev Microbiol 9:330–343
9. Miesenböck G, Angelis DAD, Rothman JE (1998) Visualizing secretion and synaptic transmission with pH-sensitive green fluorescent proteins. Nature 394:192–195
10. Medintz IL, Stewart MH, Trammell SA, Susumu K, Delehanty JB, Mei BC, Melinger JS, Blanco-Canosa JB, Dawson PE, Mattoussi H (2010) Quantum-dot/dopamine bioconjugates function as redox coupled assemblies for in vitro and intracellular pH sensing. Nat Mater 9:676–684
11. Wang XD, Stolwijk JA, Lang T, Sperber M, Meier RJ, Wegener J, Wolfbeis OS (2012) Ultra-Small, highly stable and sensitive dual nanosensors for imaging intracellular oxygen and pH in cytosol. J Am Chem Soc 134:17011–17014
12. Han JY, Burgess K (2010) Fluorescent indicators for intracellular pH. Chem Rev 110:2709–2728
13. Smith AM, Duan HW, Mohs AM, Nie SM (2008) Bioconjugated quantum dots for in vivo molecular and cellular imaging. Adv Drug Deliv Rev 60:1226–1240
14. Lewinski N, Colvin V, Drezek R (2008) Cytotoxicity of nanoparticles. Small 4:26–49
15. Albertazzi L, Storti B, Marchetti L, Beltram F (2010) Delivery and subcellular targeting of dendrimer-based fluorescent pH sensors in living cells. J Am Chem Soc 132:18158–18167
16. Gao XH, Yang LL, Petros JA, Marshal FF, Simons JW, Nie SM (2005) In vivo molecular and cellular imaging with quantum dots. Curr Opin Biotechnol 16:63–72
17. Kim HN, Guo ZQ, Zhu WH, Yoon J, Tian H (2011) Recent progress on polymer-based fluorescent and colorimetric chemosensors. Chem Soc Rev 40:79–93
18. Thomas SW, Joly GD, Swager TM (2007) Chemical sensors based on amplifying fluorescent conjugated polymers. Chem Rev 107:1339–1386
19. Feng XL, Liu LB, Wang S, Zhu DB (2010) Water-soluble fluorescent conjugated polymers and their interactions with biomacromolecules for sensitive biosensors. Chem Soc Rev 39:2411–2419
20. Tian ZY, Yu JB, Wu CF, Szymanski C, McNeill J (2010) Amplified energy transfer in conjugated polymer nanoparticle tags and sensors. Nanoscale 2:1999–2011
21. Wu CF, Chiu DT (2013) Highly fluorescent semiconducting polymer dots for biology and medicine. Angew Chem Int Ed 52:3086–3109
22. Chan YH, Wu CF, Ye FM, Jin YH, Smith PB, Chiu DT (2011) Development of ultrabright semiconducting polymer dots for ratiometric pH sensing. Anal Chem 83:1448–1455
23. Zhang Y, Hörnfeldt AB, Gronowitz S (1995) Pyridine-substituted hydroxythiophenes. IV. Preparation of 3- and 4-(2-, 3- and 4-Pyridyl)-2-hydroxythiophenes. J Heterocycl Chem 32:435–444
24. Lu G, Usta H, Risko C, Wang L, Facchetti A, Ratner MA, Marks TJ (2008) Synthesis, characterization, and transistor response of semiconducting silole polymers with substantial hole mobility and air stability. Experiment and theory. J Am Chem Soc 130:7670–7685
25. Liu H, Hao X, Duan CH, Yang H, Lv Y, Xu HJ, Wang HD, Huang F, Xiao DB, Tian ZY (2013) Al^{3+}-induced far-red fluorescence enhancement of conjugated polymer nanoparticles and its application in live cell imaging. Nanoscale 5:9340–9347
26. Yang H, Duan CH, Wu YS, Lv Y, Liu H, Lv YL, Xiao DB, Huang F, Fu HB, Tian ZY (2013) Conjugated polymer nanoparticles with Ag^{+}-sensitive fluorescence emission: a new insight into the cooperative recognition mechanism. Part Part Syst Charact 30:972–980
27. Huynh HV, He XM, Baumgartner T (2013) Halo chromic generation of white light emission using a single dithienophosphole luminophore. Chem Commun 49:4899–4901
28. Stolar M, Baumgartner T (2012) Synthesis and unexpected halochromism of carbazole-functionalized dithienophospholes. New J Chem 36:1153–1160
29. Romero-Nieto C, Durben S, Kormos IM, Baumgartner T (2009) Simple and efficient generation of white light emission from organophosphorus building blocks. Adv Funct Mater 19:3625–3631
30. Zalar P, Henson ZB, Welch GC, Bazan GC, Nguyen TQ (2012) Color tuning in polymer light-emitting diodes with lewis acids. Angew Chem Int Ed 124:7613–7616

31. Zhang X, Rehm S, Safont-Sempere MM, Würthner F (2009) Vesicular perylene dye nanocapsules as supramolecular fluorescent pH sensor systems. Nat Chem 1:623–629
32. Peng HS, Stolwijk JA, Sun LN, Wegener J, Wolfbeis OS (2010) A nanogel for ratiometric fluorescent sensing of intracellular pH values. Angew Chem Int Ed 49:4246–4249
33. Yang ZY, Qin W, Lam JWY, Chen SJ, Sung HHY, Williams ID, Tang BZ (2013) Fluorescent pH sensor constructed from a heteroatom-containing luminogen with tunable AIE and ICT characteristics. Chem Sci 4:3725–3730
34. Wen QS, Liu LB, Yang Q, Lv FT, Wang S (2013) Dopamine-modified cationic conjugated polymer as a new platform for pH sensing and autophagy imaging. Adv Funct Mater 23:764–769